REPORTS

BILAYER GRAPHENE

Electron-hole asymmetric integer and fractional quantum Hall effect in bilayer graphene

A. Kou,[1,2]* B. E. Feldman,[1]* A. J. Levin,[1] B. I. Halperin,[1] K. Watanabe,[3] T. Taniguchi,[3] A. Yacoby[1]†

The nature of fractional quantum Hall (FQH) states is determined by the interplay between the Coulomb interaction and the symmetries of the system. The distinct combination of spin, valley, and orbital degeneracies in bilayer graphene is predicted to produce an unusual and tunable sequence of FQH states. Here, we present local electronic compressibility measurements of the FQH effect in the lowest Landau level of bilayer graphene. We observe incompressible FQH states at filling factors $\nu = 2p + 2/3$, with hints of additional states appearing at $\nu = 2p + 3/5$, where $p = -2, -1, 0$, and 1. This sequence breaks particle-hole symmetry and obeys a $\nu \rightarrow \nu + 2$ symmetry, which highlights the importance of the orbital degeneracy for many-body states in bilayer graphene.

The charge carriers in bilayer graphene obey an electron-hole symmetric dispersion at zero magnetic field. Application of a perpendicular magnetic field B breaks this dispersion into energy bands known as Landau levels (LLs). In addition to the standard spin and valley degeneracy found in monolayer graphene, the $N = 0$ and 1 orbital states in bilayer graphene are also degenerate and occur at zero energy (*1*). This results in a sequence of single-particle quantum Hall states at filling factor $\nu = 4M$, where M is a nonzero integer (*2*).

When the disorder is sufficiently low, the eightfold degeneracy of the lowest LL is lifted by electron-electron interactions, which results in quantum Hall states at all integer filling factors (*3*, *4*). External electric and magnetic fields can be used to induce transitions between quantum Hall ground states with different spin and valley orders (*5*–*8*). For example, the $\nu = 0$ state, which is a canted antiferromagnet at large perpendicular magnetic field, can be tuned into a ferromagnetic state by a large parallel magnetic field, or a layer-polarized state under large perpendicular electric field (*5*–*11*). The order in which orbital states are filled remains an open question, with suggestions of full polarization or orbitally coherent states, depending on system parameters (*12*–*16*). The interplay between externally applied fields and intrinsic electron-electron interactions, both of which break the degeneracies of bilayer graphene, produces a rich phase diagram.

Knowledge of the ground state at integer filling factors is especially important for investigating the physics of partially filled LLs, where, in exceptionally clean samples, the charge carriers condense into fractional quantum Hall (FQH) states. The above-mentioned degrees of freedom, as well as the strong screening of the Coulomb interaction in bilayer graphene, are expected to result in an interesting sequence of FQH states in the lowest LL (*16*–*21*). Partial breaking of the SU(4) symmetry in monolayer graphene has already resulted in sequences of FQH states with multiple missing fractions (*22*–*26*).

The few FQH states reported in bilayer graphene thus far include hints of a $\nu = 1/3$ state (*27*) and robust FQH states at $\nu = -1/2$ and $-4/3$ in suspended samples (*28*). Here, we report local compressibility measurements, performed using a scanning single-electron transistor (*29*, *30*), of a bilayer graphene device fabricated on hexagonal boron nitride (h-BN). An optical image of the contacted device is shown in Fig. 1A.

Figure 1B shows a measurement of the inverse compressibility $d\mu/dn$ as a function of filling factor at $B = 2$ T. Incompressible features are present at all nonzero multiples of $\nu = 4$, as expected for bilayer graphene. The full width at half maximum of the $\nu = 4$ peak provides a measure of the disorder in the system and is on the order of 10^{10} cm^{-2}, similar to that observed in suspended bilayers (*3*, *31*). Broken-symmetry states at $\nu = 0$ and ± 2 are also visible at $B = 2$ T, which further indicates the cleanliness of the sample. In Fig. 1B, the inverse compressibility appears more negative for $|\nu| < 4$ than in higher LLs, and we explore this behavior further by averaging the inverse compressibility between 8 and 11.5 T, which reduces fluctuations caused by localized states (Fig. 1C). The background inverse compressibility between integer quantum Hall states is close to zero at $4 < \nu < 8$ but is markedly more negative for $0 < \nu < 4$, qualitatively consistent with observations in the lowest LL in monolayer graphene (*26*, *32*, *33*).

Even within the lowest LL, the background inverse compressibility has two different characteristic shapes. It is more negative and less flat when increasing the filling factor from an even value than from an odd value. One might expect that as states are filled with electrons from an even filling factor, electron-electron interactions break the degeneracy between the $N = 0$ and 1 orbital LLs, so that only the $N = 0$ LL is occupied. When states are filled with electrons from an odd filling factor, the $N = 0$ LL is already full, so electrons start to occupy the $N = 1$ LL. The more negative background inverse compressibility between $\nu = 0$ and 1 and between $\nu = 2$ and 3 points to the presence of less screening or more electron-electron correlations in the

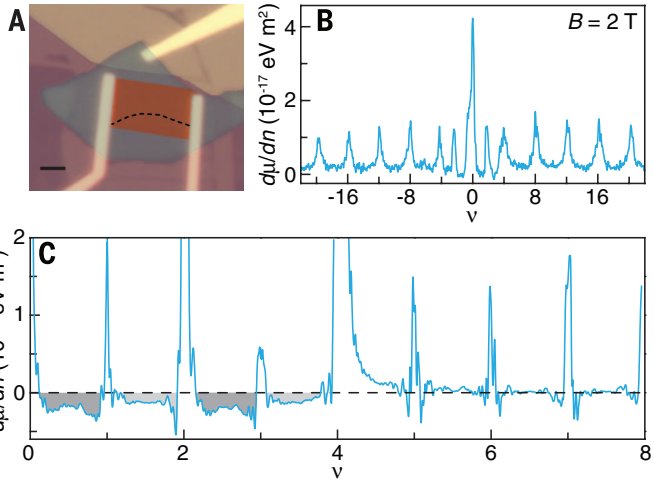

Fig. 1. Sample image and characterization. (**A**) Optical image of the device with colored overlays showing the graphite (blue), boron nitride (purple), and monolayer-bilayer graphene hybrid (red). The dashed line marks the interface between monolayer and bilayer graphene. Scale bar, 2 μm. (**B**) Inverse compressibility $d\mu/dn$ as a function of filling factor ν at magnetic field $B = 2$ T. (**C**) Average inverse compressibility between $B = 8$ and 11.5 T as a function of filling factor after current annealing to 4 V. Shaded areas indicate regions of more negative background inverse compressibility.

[1]Department of Physics, Harvard University, Cambridge, MA 02138, USA. [2]Department of Applied Physics, Yale University, New Haven, CT 06520, USA. [3]National Institute for Materials Science, Tsukuba, Japan.
*These authors contributed equally to this work. †Corresponding author. E-mail: yacoby@physics.harvard.edu

N = 0 LL when compared with the N = 1 LL with an underlying filled N = 0 LL.

Figure 2, A and C, shows the inverse compressibility as a function of filling factor and magnetic field after we further cleaned the sample by current annealing. Quantum Hall states appear as vertical features when plotted in this form, whereas localized states, which occur at a constant density offset from their parent states, curve as the magnetic field is changed (*26*, *34*). We can then unambiguously identify the incompressible states that appear at ν = −10/3, −4/3, 2/3, and 8/3 as FQH states. These states follow a $\nu = 2p + 2/3$ sequence, where p = −2, −1, 0, and 1. Above 10 T, we also see evidence of developing states at ν = −17/5, −7/5, 3/5, and 13/5, which follow a similar $\nu = 2p + 3/5$ sequence. The FQH states closer to the charge-neutrality point are more incompressible than those at higher filling factors, and they persist to fairly low magnetic fields, with the last hints disappearing around 6 T.

The line plots in Fig. 2, B and D, show the average inverse compressibility in each filling factor range from 7.9 to 11.9 T. The plots highlight the FQH states identified above, as well as the different behaviors exhibited by the inverse compressibility, which shows especially strong divergences as the filling factor is increased from ν = 0 and 2. Similar to $\nu > 0$, the background inverse compressibility at negative filling factors displays an even-odd effect with more negative values when increasing the filling factor from an even integer. The FQH states coincide with areas of more negative background inverse compressibility, consistent with its attribution to Coulomb interactions (*32*, *35*). Despite theoretical predictions of robust FQH states in the N = 2 LL and experimental hints in other samples (*8*), we do not observe any FQH states between $|\nu| = 4$ and 8.

Notably, the observed sequence of FQH states and the background inverse compressibility pattern break particle-hole symmetry and instead follow a $\nu \rightarrow \nu + 2$ pattern. The $\nu \rightarrow \nu + 2$ symmetry indicates that the orbital degeneracy is playing an important role. This symmetry was predicted based on a model that incorporates the strong screening and LL mixing present in the lowest LL of bilayer graphene (*16*). The absence of FQH states between ν = −3 and −2 or in the intervals connected to $-3 < \nu < -2$ by $\nu \rightarrow \nu + 2$ symmetry suggests a difference in electron-electron interactions between partial filling when both the N = 0 and 1 LLs are empty and partial filling of the N = 1 LL when the N = 0 LL is full. The increased LL mixing present when the N = 0 LL is full (*36*) may be weakening the strength of FQH states in the N = 1 LL.

Our observed FQH sequence also suggests possible orbital polarization of the FQH states. The FQH states we observe at $\nu = 2p + 2/3$ could be singlet-like states of N = 0 and 1 orbitals or could arise from a ν = 2/3 state with full orbital polarization. The next strongest FQH states that we observe occur at $\nu = 2p + 3/5$, which must have some nonzero orbital polarization. The strongest FQH states at multiples of ν = 1/5 do not have even numerators, in contrast to recent theoretical predictions (*16*).

The FQH states that we observe are different from those seen in previous experiments on bilayer graphene, which may point to different patterns of symmetry-breaking in the different systems. In (*28*), FQH states at ν = −4/3 and −1/2 were observed, with hints of additional features at ν = −8/5 and −2/3; the only FQH state seen in both devices is ν = −4/3. It is also possible that the effective interactions present in the two samples may be different because of the differences in screening between a suspended bilayer and a bilayer on a substrate. The fact that different sample preparations result in different FQH states could be a sign of the theoretically predicted tunability of the FQH effect in bilayer graphene (*17*, *19*, *21*). Applying a perpendicular electric and/or a parallel magnetic field to the sample may provide insight into the conditions under which different FQH states are favored. We can contrast this with monolayer graphene, in which both suspended and substrate-supported samples have shown similar sequences of FQH states (*22*–*26*, *37*). Though phase transitions of FQH states were observed (*38*) in monolayers, these involved changes in only the spin and/or valley polarization; the sequence of observed FQH states did not change. In bilayer graphene, however, it appears that the sample geometry and/or substrate play an important role in determining the relative strengths of various incompressible FQH states.

We can integrate the inverse compressibility with respect to density to obtain the energy cost of adding an electron to the system (*26*). This quantity must be divided by the quasi-particle charge associated with each state to determine the corresponding energy gap Δ_ν. The most likely quasi-particle charge for states at multiples of ν = 1/3 is $e/3$ (where e is the charge of an electron), but the nature of the FQH states in bilayer graphene is not yet fully understood, so we plot the extracted steps in chemical potential $\Delta\mu_\nu$ in Fig. 3A. For ν = −4/3 and 2/3, $\Delta\mu_\nu$ is ~0.75 and ~0.6 meV, respectively, at B = 12 T. Assuming a quasi-particle charge of $e/3$, the energy gap we

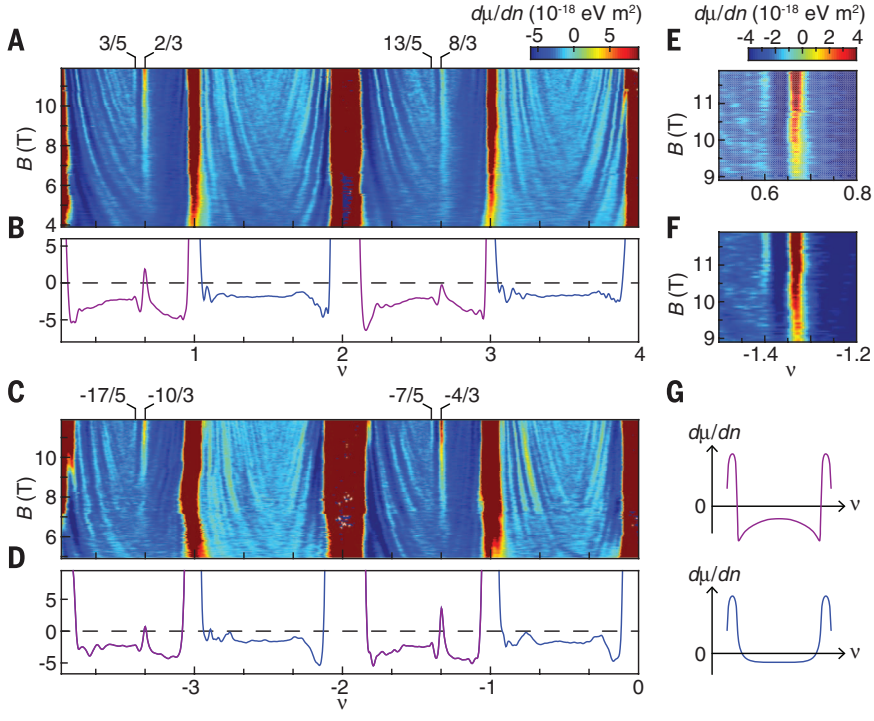

Fig. 2. Fractional quantum Hall states in bilayer graphene. (**A** and **C**) Inverse compressibility as a function of filling factor and magnetic field. The color scales are the same in both panels. (**B** and **D**) Average inverse compressibility between B = 7.9 and 11.9 T as a function of filling factor. Colors indicate regions of similar behavior in the background inverse compressibility. (**E** and **F**) Inverse compressibility as a function of filling factor and magnetic field near ν = −7/5 and 3/5. (**G**) Diagram highlighting the differences in background inverse compressibility between $\nu = 2p$ and $\nu = 2p + 1$ in purple and $\nu = 2p + 1$ and $\nu = 2p$ in blue.

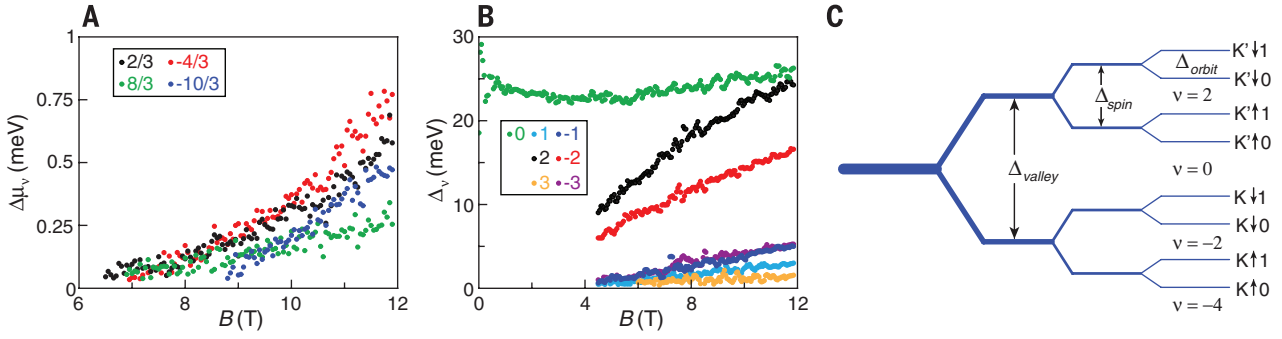

Fig. 3. Steps in chemical potential. (**A**) Steps in chemical potential of the fractional quantum Hall states as a function of magnetic field. (**B**) Energy gaps of the integer broken-symmetry states in the lowest LL. (**C**) Diagram showing the order of symmetry-breaking in the sample. K and K′ denote the valleys of bilayer graphene.

find at $\nu = -4/3$ is comparable with, if somewhat larger than, that found in (*28*) at similar magnetic fields. The gaps of FQH states further away from charge neutrality are smaller; $\Delta\mu_{-10/3}$ and $\Delta\mu_{8/3}$ are only ~0.5 and ~0.3 meV, respectively, at $B = 12$ T. All of the extracted gaps increase monotonically with B. The gaps appear to scale approximately linearly or, in some cases, even superlinearly with field, although we cannot explicitly rule out a $\sqrt{B}$-dependence of the gaps at $\nu = 8/3$ and $-10/3$. Previous measurements of broken-symmetry integer states in suspended bilayers revealed a linear B dependence of the gaps, which was attributed to LL mixing (*31*, *39*). The magnitude of the FQH energy gaps is probably sensitive to the details of disorder in the system and perhaps also to the ratio between magnetic length and sample-gate distance.

The energy gaps of the integer filling factors $|\nu| < 4$ are shown in Fig. 3B. All of the gaps increase with B, except for $\nu = 0$, which is fairly constant around 23 to 25 meV over almost the full range in the magnetic field. Around 4 T, the gap dips slightly before increasing again at $B = 0$ T. The size of the gap and its persistence to zero field lead us to conclude that the ground state at $\nu = 0$ is layer-polarized. If we assume that the $\nu \rightarrow \nu + 2$ symmetry arises from the orbital degree of freedom, we can fully determine the sequence of symmetry-breaking in the sample (Fig. 3C): valley polarization is first maximized, then spin polarization, and finally orbital polarization. The large valley polarization in our sample relative to other bilayer devices may be caused by interactions with the substrate (*40*). Large band gaps have been observed in monolayer graphene samples on h-BN with a proximal gate, which have been attributed to the breaking of sublattice symmetry by h-BN or screening from the nearby metal (*37*, *41*, *42*). It is also possible that the difference in distance between the top layer to the graphite gate and the bottom layer to the graphite gate is creating a potential difference in the two layers (*43*), or that the different environments experienced by each layer play a role. Even if the $\nu = 0$ gap is caused by single-particle effects, its constancy over our entire field range is somewhat surprising because both the potential difference between the layers and the Coulomb energy are expected to contribute to the gap (*44*).

Local measurement allows us to probe multiple locations on the sample, and although we do observe fluctuations in the strengths of the broken-symmetry and FQH states, the overarching pattern of FQH states is consistent across the entire sample (fig. S1) and also did not change with current annealing (fig. S2). The electron-hole asymmetric sequence of FQH states can therefore be attributed to the intrinsic properties of bilayer graphene, rather than disorder or other local effects. The observation of an unconventional sequence of FQH states in bilayer graphene indicates the importance of its underlying symmetries and opens avenues for exploring the nature and tunability of the FQH effect.

REFERENCES AND NOTES

1. E. McCann, V. I. Fal'ko, *Phys. Rev. Lett.* **96**, 086805 (2006).
2. K. S. Novoselov *et al.*, *Nat. Phys.* **2**, 177–180 (2006).
3. B. E. Feldman, J. Martin, A. Yacoby, *Nat. Phys.* **5**, 889–893 (2009).
4. Y. Zhao, P. Cadden-Zimansky, Z. Jiang, P. Kim, *Phys. Rev. Lett.* **104**, 066801 (2010).
5. R. T. Weitz, M. T. Allen, B. E. Feldman, J. Martin, A. Yacoby, *Science* **330**, 812–816 (2010).
6. S. Kim, K. Lee, E. Tutuc, *Phys. Rev. Lett.* **107**, 016803 (2011).
7. J. Velasco Jr. *et al.*, *Nat. Nanotechnol.* **7**, 156–160 (2012).
8. P. Maher *et al.*, *Nat. Phys.* **9**, 154–158 (2013).
9. M. Kharitonov, *Phys. Rev. Lett.* **109**, 046803 (2012).
10. E. V. Gorbar, V. P. Gusynin, V. A. Miransky, I. A. Shovkovy, *Phys. Rev. B* **85**, 235460 (2012).
11. J. Lambert, R. Côté, *Phys. Rev. B* **87**, 115415 (2013).
12. Y. Barlas, R. Côté, K. Nomura, A. H. MacDonald, *Phys. Rev. Lett.* **101**, 097601 (2008).
13. R. Côté, J. Lambert, Y. Barlas, A. H. MacDonald, *Phys. Rev. B* **82**, 035445 (2010).
14. K. Shizuya, *Phys. Rev. B* **86**, 045431 (2012).
15. C. Töke, *Phys. Rev. B* **88**, 241411 (2013).
16. Z. Papić, D. A. Abanin, *Phys. Rev. Lett.* **112**, 046602 (2014).
17. V. M. Apalkov, T. Chakraborty, *Phys. Rev. Lett.* **105**, 036801 (2010).
18. Z. Papić, R. Thomale, D. A. Abanin, *Phys. Rev. Lett.* **107**, 176602 (2011).
19. Z. Papić, D. A. Abanin, Y. Barlas, R. N. Bhatt, *Phys. Rev. B* **84**, 241306(R) (2011).
20. V. M. Apalkov, T. Chakraborty, *Phys. Rev. Lett.* **107**, 186803 (2011).
21. K. Snizhko, V. Cheianov, S. H. Simon, *Phys. Rev. B* **85**, 201415(R) (2012).
22. X. Du, I. Skachko, F. Duerr, A. Luican, E. Y. Andrei, *Nature* **462**, 192–195 (2009).
23. F. Ghahari, Y. Zhao, P. Cadden-Zimansky, K. Bolotin, P. Kim, *Phys. Rev. Lett.* **106**, 046801 (2011).
24. C. R. Dean *et al.*, *Nat. Phys.* **7**, 693–696 (2011).
25. D. S. Lee, V. Skákalová, R. T. Weitz, K. von Klitzing, J. H. Smet, *Phys. Rev. Lett.* **109**, 056602 (2012).
26. B. E. Feldman, B. Krauss, J. H. Smet, A. Yacoby, *Science* **337**, 1196–1199 (2012).
27. W. Bao *et al.*, *Phys. Rev. Lett.* **105**, 246601 (2010).
28. D.-K. Ki, V. I. Fal'ko, A. F. Morpurgo, *Nano Lett.* **14**, 2135–2139 (2014).
29. M. J. Yoo *et al.*, *Science* **276**, 579–582 (1997).
30. A. Yacoby, H. F. Hess, T. A. Fulton, L. N. Pfeiffer, K. W. West, *Solid State Commun.* **111**, 1–13 (1999).
31. J. Martin, B. E. Feldman, R. T. Weitz, M. T. Allen, A. Yacoby, *Phys. Rev. Lett.* **105**, 256806 (2010).
32. G. L. Yu *et al.*, *Proc. Natl. Acad. Sci. U.S.A.* **110**, 3282–3286 (2013).
33. B. Skinner *et al.*, *Phys. Rev. B* **88**, 155417 (2013).
34. S. Ilani *et al.*, *Nature* **427**, 328–332 (2004).
35. J. P. Eisenstein, L. N. Pfeiffer, K. W. West, *Phys. Rev. Lett.* **68**, 674–677 (1992).
36. M. R. Peterson, C. Nayak, *Phys. Rev. B* **87**, 245129 (2013).
37. B. Hunt *et al.*, *Science* **340**, 1427–1430 (2013).
38. B. E. Feldman *et al.*, *Phys. Rev. Lett.* **111**, 076802 (2013).
39. R. Nandkishore, L. Levitov, *Phys. Rev. Lett.* **104**, 156803 (2010).
40. Supplementary materials are available on *Science* Online.
41. F. Amet, J. R. Williams, K. Watanabe, T. Taniguchi, D. Goldhaber-Gordon, *Phys. Rev. Lett.* **110**, 216601 (2013).
42. L. A. Ponomarenko *et al.*, *Nat. Phys.* **7**, 958–961 (2011).
43. E. McCann, *Phys. Rev. B* **74**, 161403(R) (2006).
44. C. Töke, V. I. Fal'ko, *Phys. Rev. B* **83**, 115455 (2011).

ACKNOWLEDGMENTS

We thank D. A. Abanin, R. Hegde, A. H. MacDonald, B. Skinner, and I. Sodemann for useful discussions and J. D. Sanchez-Yamagishi for help with fabrication. This work is partially supported by the U.S. Department of Energy (DOE), Office of Basic Energy Sciences, Division of Materials Sciences and Engineering under award no. DE-SC0001819. Device optimization and initial measurements were supported by the 2009 U.S. Office of Naval Research Multidisciplinary University Research Initiative on Graphene Advanced Terahertz Engineering (Gate) at the Massachusetts Institute of Technology, Harvard University, Boston University, and the Nanoelectronics Research Initiative–South West Academy of Nanoelectronics program. This material is based, in part, on work supported by the Science and Technology Center for Integrated Quantum Materials, under NSF grant DMR-1231319. Devices were fabricated at the Center for Nanoscale Systems at Harvard University, supported by NSF under grant ECS-0335765. A.K. acknowledges support from the DOE Office of Science Graduate Fellowship Program. A.J.L. is supported through a fellowship from the U.S. Department of Defense (National Defense Science and Engineering Graduate Fellowship program).

SUPPLEMENTARY MATERIALS

www.sciencemag.org/content/345/6192/55/suppl/DC1
Materials and Methods
Supplementary Text
Figs. S1 to S3
References (*45*, *46*)

30 December 2013; accepted 20 May 2014
Published online 29 May 2014;
10.1126/science.1250270

Electron-hole asymmetric integer and fractional quantum Hall effect in bilayer graphene

A. Kou *et al.*

Science **345**, 55 (2014);
DOI: 10.1126/science.1250270